Supporting Information

Suppressing thermal-quenching of lead halide perovskite nanocrystals by constructing wide-bandgap surface layer for achieving thermally stable white light-emitting diodes

Qinggang Zhang,[a,b] Mengda He,[a] Qun Wan,[a] Weilin Zheng,[a] Mingming Liu,[a] Congyang Zhang,[a] Xinrong Liao,[a] Wenji Zhan,[a] Long Kong,[a] Xiaojun Guo,[b] Liang Li,*[a,c]

[a] School of Environmental Science and Engineering, Shanghai Jiao Tong University, Shanghai 200240, China

[b] Department of Electronic Engineering, School of Electronics Information and Electrical Engineering, Shanghai Jiao Tong University, Shanghai 200240, China

[c] Shanghai Engineering Research Center of Solid Waste Treatment and Resource Recovery, Shanghai Jiao Tong University, Shanghai 200240, China

Corresponding Author: liangli117@sjtu.edu.cn

Experimental Section

Materials.

Cesium bromide (CsBr, 99.5%), lead bromide ($PbBr_2$, 99%), potassium sulfate (K_2SO_4, 99.9%), potassium bromide (KBr, 99%), potassium hydroxide (KOH, 85%) were purchased from Aladdin. Potassium fluoride (KF, 99%) was purchased from Adamas. Mesoporous SiO_2 template (MCM-41) was purchased from Tianjin Yuanli Chemical Co., Ltd. All the chemicals were used without further purification.

Preparation of pristine $CsPbBr_3$ nanocrystals.

The pristine $CsPbBr_3$ NCs were synthesized using a high temperature solid-state reaction. Briefly, CsBr (127.7 mg, 0.6 mmol) and $PbBr_2$ (221.4 mg, 0.6 mmol) were added to a beaker with 50 mL ultrapure water and stirred constantly under heating conditions to form a clear solution. Then, a certain amount of mesoporous SiO_2 templates (MCM-41 molecular sieve, 1047 mg) was added to the above solution with continuous stirring, and then dried at 80 °C. Then, the obtained mixture was ground and calcined at 700 °C for 30 min with a heating rate of 5 °C min^{-1} in the tubular furnace in argon atmosphere. After cooling to room temperature, the obtained sample was washed with ultrapure water for several times to remove incompletely encapsulated $CsPbBr_3$ NCs or other salts on the surface of SiO_2. Finally, the washed sample was fully dried at 60°C, and the product was named pristine $CsPbBr_3$.

Preparation of anions-treated $CsPbBr_3$ nanocrystals.

Taking SO_4^{2-}-treated $CsPbBr_3$ NCs as example, the process of obtaining $CsPbBr_3$-SO_4 by the modified high temperature solid-state reaction was as follows. CsBr (127.7 mg, 0.6 mmol) and $PbBr_2$ (221.4 mg, 0.6 mmol) were added to a beaker with 50 mL ultrapure water and stirred constantly under heating conditions to form a clear solution. Then, a certain amount of mesoporous SiO_2 templates (MCM-41 molecular sieve, 1047 mg) was added to the above solution with continuous stirring at 80 °C. Next, a certain amount of K_2SO_4 aqueous solution was slowly add into the above mixed solution, and the mixture was stirred for more than three hour to obtain a solid powder. The obtained solid powder was ground and calcined at 700 °C for 30 min with a heating rate of 5 °C

min^{-1} in the tubular furnace in argon atmosphere. After cooling to room temperature, the obtained sample was washed with ultrapure water for several times to remove incompletely encapsulated $CsPbBr_3$ NCs or other salts on the surface of SiO_2. Finally, the washed sample was fully dried at 60°C, and the product was denoted as $CsPbBr_3$-SO_4.

In this case, the mole ratio of CsBr and $PbBr_2$ was always kept at 1:1. And the concentration of SO_4^{2-} ion depends on the mole ratio of SO_4^{2-}: $CsPbBr_3$ from 0% to 100%.

Other passivation ions, such as F^-, OH^-, Br^-, can also be achieved by changing the type of potassium salt (KF, KOH, KBr) under the same experimental conditions.

Preparation of colloidal $CsPbBr_3$ NCs.

2 mmol $PbBr_2$, 20 mL 1-octadecene (ODE), 5 mL oleylamine (OAm), 5 mL oleic acid (OA) were added into a 100 mL three-neck flask and evacuated for 30 min at 120 °C. Then, the temperature raised to 180 °C under argon atmosphere until $PbBr_2$ salt had completely dissolved. Afterward, 1 mL of CsOA precursor (0.5 M), which was pre-heated at 70°C, was injected into the above solution. After 10 s, the three-neck flask was placed in an ice-water bath and cooled to room temperature. Equal methyl acetate was added into the crude solution and precipitated via centrifugation at 10000 rpm. The precipitate was dispersed in 30 mL toluene solution.

Preparation of anions-treated colloidal $CsPbBr_3$ NCs.

In this procedure, 1 mmol potassium salts (such as KBr, K_2SO_4, KF) was added into 5 mL of the purified $CsPbBr_3$ NCs (~10 mg mL^{-1}). Next, the mixture was stirred for 30 min at room temperature. After treatment, the anions-treated colloidal $CsPbBr_3$ NCs solution was collected via centrifugation.

Thermal quenching experiments.

For temperature-dependent PL measurements, the solid powder samples, including pristine $CsPbBr_3$ NCs and different anions-treated $CsPbBr_3$ NCs, were respectively covered on the bottom of the glass bottle, which were then placed on heating plate. *In situ* PL spectra were recorded at a specific temperatures in the range of 293-373 K, which were used to evaluate the thermal quenching behaviors of NCs.

PLQY Measurements.

The absolute PLQYs of the $CsPbBr_3$ NCs powders were measured based on the Edinburgh FLS1000 pectrophotometer with integrating sphere.

Fabrication of the white LED device.

First, green-emitting $CsPbBr_3$ NCs powders and red-emitting commercial KSF phosphors were mixed with a certain amount of UV-cured optical adhesive. To remove the bubbles from the optical adhesive, the resulting mixtures were heated at 40 °C for 0.5 h under vacuum. After that, the mixtures were deposited on a 450 nm GaN LED chip and then UV cured for 50 s, then the WLED was obtained.

Structural characterization.

The powder X -ray diffraction (XRD) patterns of samples were performed by a Bruker D8 Advance X-ray Diffractometer at 40 kV and 30 mA using Cu K_α radiation (λ=1.5406 Å). The morphologies and elemental distributions and high-angle annular dark−field scanning transmission electron microscopy (HAADF−STEM) images were analyzed by Mira3/MIRA3 (SEM) field emission scanning electron microscope (FESEM) and FEI (TALOS F200X) transmission electron microscope (TEM) instruments. PL spectra of the samples were recorded on an Ocean Optics LS-450 spectrometer and a fluorescence spectrometer (HAAS-2000). UV-Vis absorption spectra were measured by a UV-Vis spectrophotometer (PerkinElmer Lambda 950). The surface composition and chemical state of the samples were detected through XPS analysis using a Kratos Axis Ultra DLD instrument. The PL decay curves were recorded on an Edinburgh FLS1000 spectrophotometer with the excitation wavelength at 365 nm. Fourier transform infrared (FT-IR) spectra were measured by Fourier infrared spectrometer (Nicolet 6700). Raman spectra were measured by the confocal micro Raman spectrometer (inVia Qontor). The *in-situ* characterizations involved in this work were based on the above equipment, and the heating rate of additional temperature control equipment was 10 K min^{-1}.

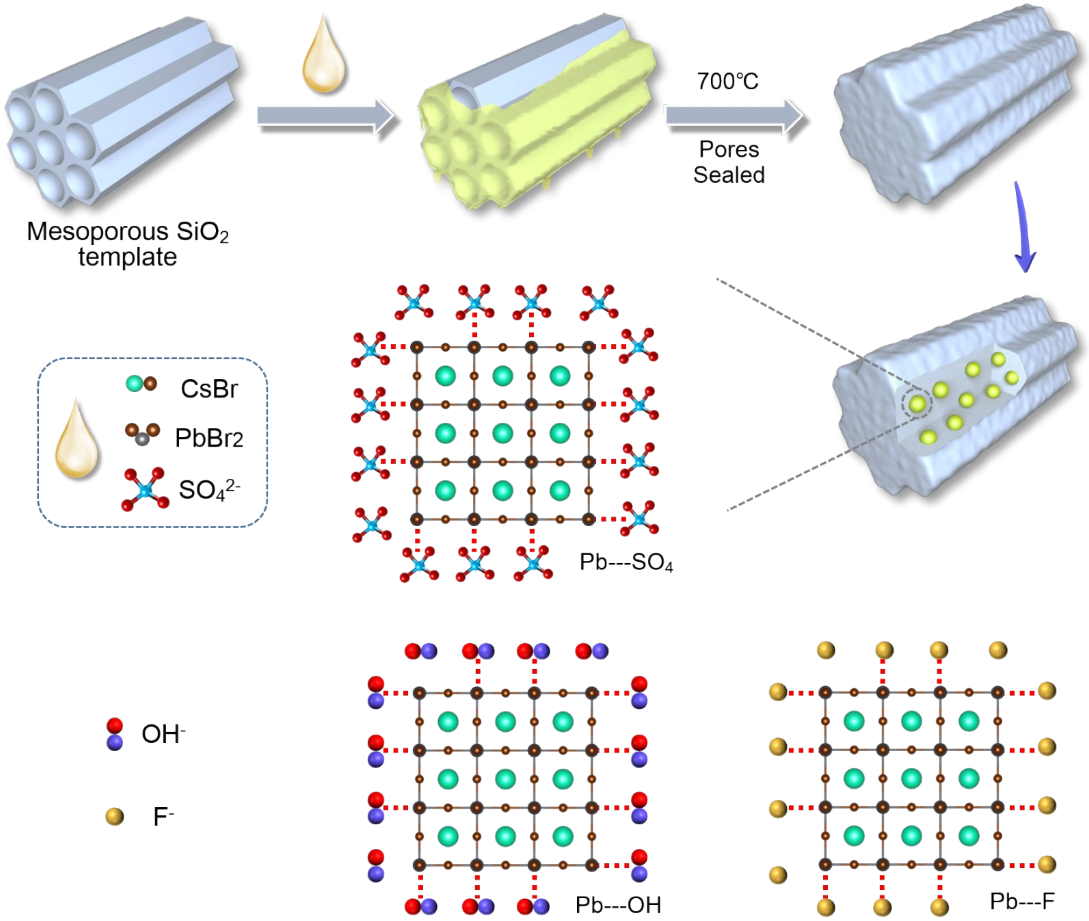

Figure S1. Synthetic route of anions-treated $CsPbBr_3$ NCs in high-temperature solid-state method.

To guarantee the accuracy of the data, we analyzed three locations in each sample, including original $CsPbBr_3$ NCs, $CsPbBr_3$-SO_4, $CsPbBr_3$-F, $CsPbBr_3$-OH. The results showed that the content of perovskite nanocrystals encapsulated into SiO_2 was about 18 wt% (**Table S1-4**).

Table S1. EDS of Cs, Pb, Br, O and Si for pristine $CsPbBr_3$ NCs samples

Sample	O/at%	Si/at%	Br/at%	Cs/at%	Pb/at%
$CsPbBr_3$	67.61	30.14	0.82	0.74	0.69
	66.49	30.50	1.11	1.06	0.85
	65.82	30.87	1.27	1.03	1.02
Mean/at%	**66.64**	**30.50**	**1.07**	**0.94**	**0.85**
Sample	O/wt%	Si/wt%	Br/wt%	Cs/wt%	Pb/wt%
$CsPbBr_3$	48.41	37.87	2.94	4.40	6.39
	45.76	36.84	3.81	6.04	7.55
	44.46	36.60	4.27	5.80	8.88
Mean/wt%	**46.21**	**37.10**	**3.67**	**5.41**	**7.61**

Table S2. EDS of Cs, Pb, Br, S, O and Si for SO_4^{2-} treated $CsPbBr_3$ NCs samples

Sample	O/at%	Si/at%	S/at%	Br/at%	Cs/at%	Pb/at%
$CsPbBr_3$-SO_4	64.48	30.95	0.30	2.47	0.85	0.95
	64.45	30.69	0.35	2.64	0.86	1.01
	64.47	31.20	0.41	1.89	1.14	0.89
Mean/at%	**64.47**	**30.92**	**0.36**	**2.34**	**0.95**	**0.96**
Sample	O/wt%	Si/wt%	S/wt%	Br/wt%	Cs/wt%	Pb/wt%
$CsPbBr_3$-SO_4	42.68	35.95	0.40	8.16	4.66	8.14
	42.28	35.34	0.46	8.64	4.67	8.60
	42.82	36.37	0.54	6.28	6.30	7.69
Mean/wt%	**42.59**	**35.89**	**0.47**	**7.69**	**5.21**	**8.15**

Table S3. EDS of Cs, Pb, Br, F, O and Si for F^- treated $CsPbBr_3$ NCs samples

Sample	O/at%	Si/at%	F/at%	Br/at%	Cs/at%	Pb/at%
$CsPbBr_3$-F	66.48	30.04	0.62	1.32	0.86	0.67
	65.87	30.48	0.56	1.53	0.94	0.60
	67.27	29.49	0.48	1.18	0.83	0.74
Mean/at%	**66.54**	**30.00**	**0.56**	**1.35**	**0.88**	**0.67**
Sample	O/wt%	Si/wt%	F/wt%	Br/wt%	Cs/wt%	Pb/wt%
$CsPbBr_3$-F	46.69	37.04	0.52	4.62	5.04	6.08
	45.97	37.35	0.47	5.34	5.46	5.42
	47.35	36.44	0.40	4.16	4.86	6.78
Mean/wt%	**46.67**	**36.94**	**0.46**	**4.72**	**5.12**	**6.09**

Table S4. EDS of Cs, Pb, Br, O and Si for OH^- treated $CsPbBr_3$ NCs samples

Sample	O/at%	Si/at%	Br/at%	Cs/at%	Pb/at%
$CsPbBr_3$-OH	67.38	28.93	1.66	1.03	1.00
	66.00	31.04	1.26	0.93	0.77
	67.93	28.60	1.29	1.14	1.04
Mean/at%	**67.10**	**29.52**	**1.41**	**1.03**	**0.94**
Sample	O/wt%	Si/wt%	Br/wt%	Cs/wt%	Pb/wt%
$CsPbBr_3$-OH	45.56	34.34	5.60	5.79	8.72
	45.67	37.70	4.35	5.34	6.94
	46.05	34.04	4.38	6.40	9.13
Mean/wt%	**45.76**	**35.36**	**4.78**	**5.84**	**8.26**

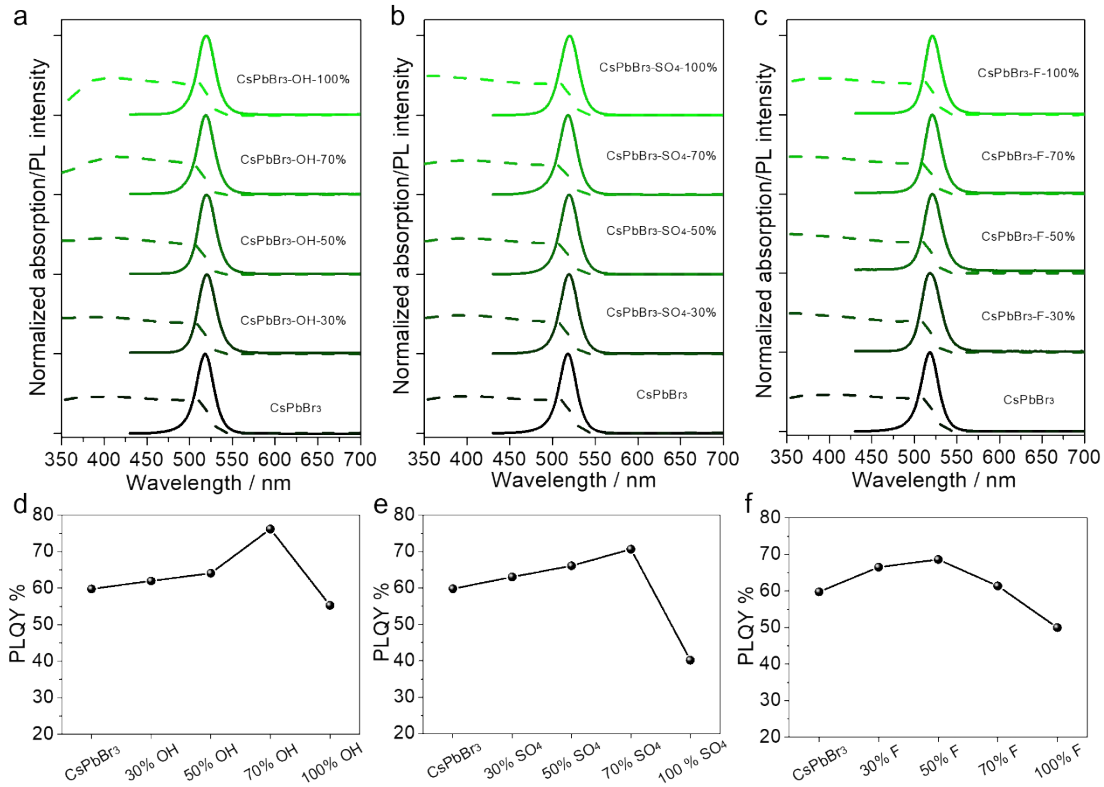

Figure S2. PL spectra (solid lines, excitation wavelength is 365 nm) and optical absorption (dashed lines) of pristine and different anions treated $CsPbBr_3$ NCs: (a) $CsPbBr_3$-OH NCs, (b) $CsPbBr_3$-SO_4 NCs, (c) $CsPbBr_3$-F NCs. Absolute PLQYs of $CsPbBr_3$ NCs with different anions treatment: (d) $CsPbBr_3$-OH NCs, (e) $CsPbBr_3$-SO_4 NCs, (f) $CsPbBr_3$-F NCs.

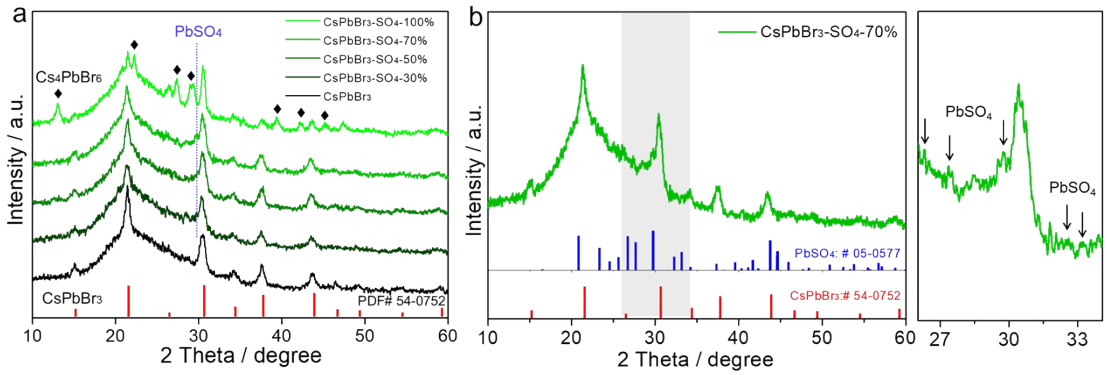

Figure S3. XRD patterns of $CsPbBr_3$ NCs with different SO_4^{2-} ions treatment.

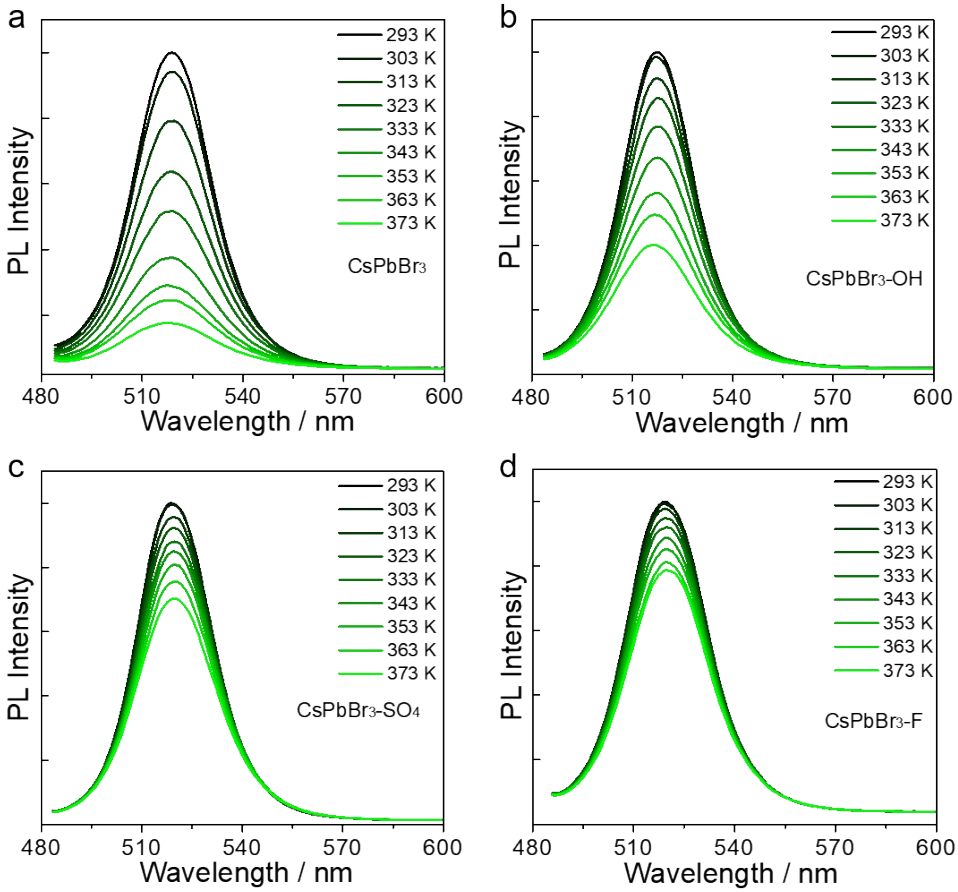

Figure S4. *In situ* PL spectra of pristine $CsPbBr_3$ NCs (a), $CsPbBr_3$-OH NCs (b), $CsPbBr_3$-SO_4 NCs (c), $CsPbBr_3$-F NCs (d), at increasing temperature from 293K to 373K.

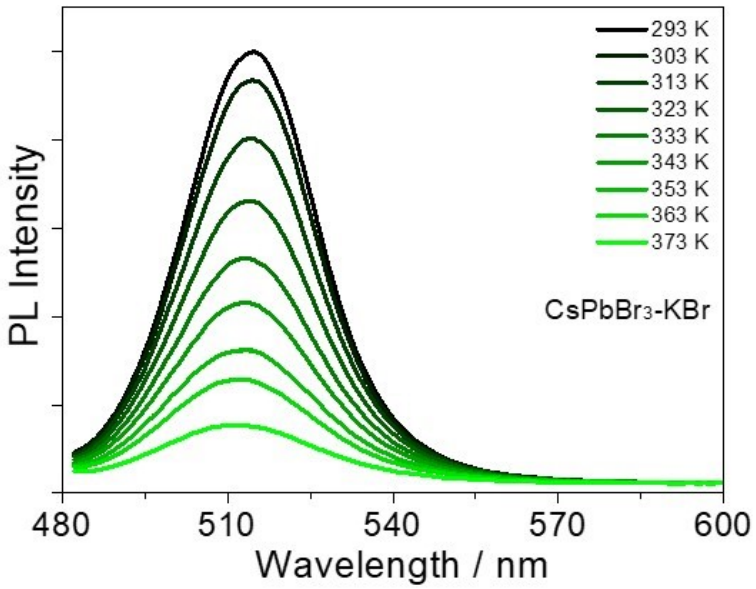

Figure S5. *In situ* PL spectra of KBr-treated $CsPbBr_3$ NCs at increasing temperature from 293K to 373K.

Table S5. ΔE_{trap} values of different anions treated $CsPbBr_3$ NCs.

Samples	$CsPbBr_3$	$CsPbBr_3$-OH	$CsPbBr_3$-SO_4	$CsPbBr_3$-F
$\triangle E_{trap}$/meV	396	437	489	501

Table S6. Formation energy of different lead compounds.

Samples	$PbBr_2$	$Pb(OH)_2$	$PbSO_4$	PbF_2
$\triangle E_{form}$/eV	-0.91	-1.25	-2.03	-2.68

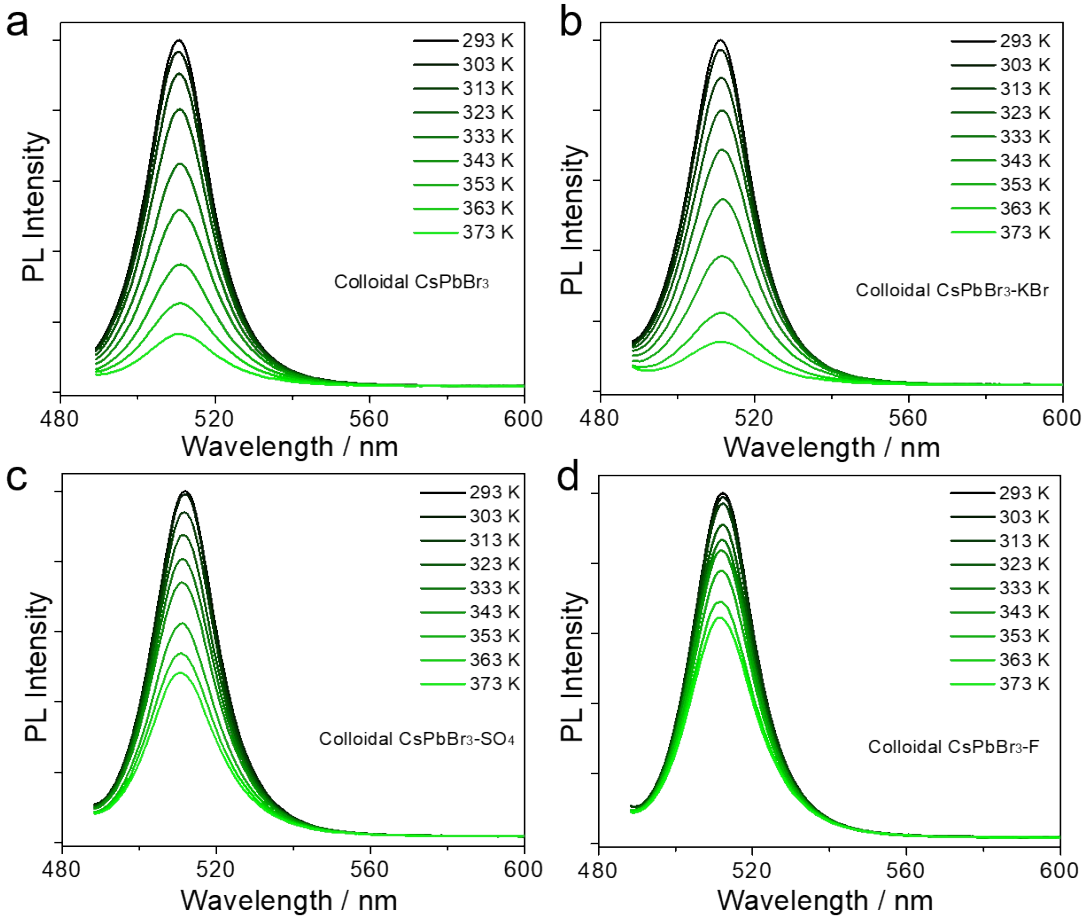

Figure S6. *In situ* PL spectra of pristine colloidal $CsPbBr_3$ NCs (a), colloidal $CsPbBr_3$-KBr NCs (b), colloidal $CsPbBr_3$-SO_4 NCs (c), colloidal $CsPbBr_3$-F NCs (d), at increasing temperature from 293K to 373K.

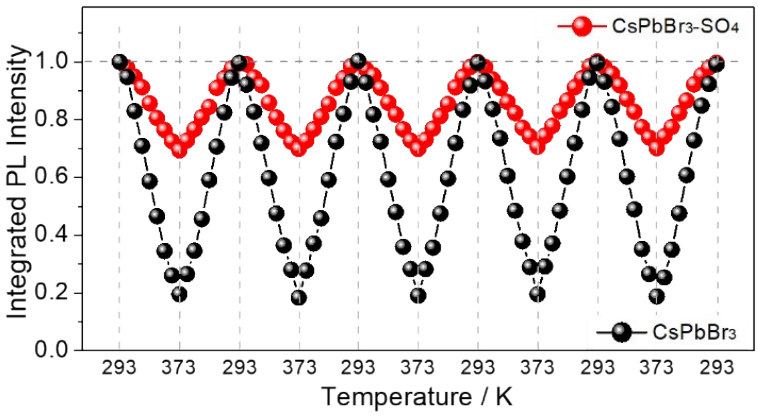

Figure S7. Integrated PL intensity of pristine and SO_4^{2-}-treated $CsPbBr_3$ during five thermal cycles between T = 293 and 373 K.

Table S7. The fitting parameters of the decay curves for pristine $CsPbBr_3$ NCs at increasing temperature from 293 to 373 K.

Temperature / K	A_1 (%)	τ_1 (ns)	A_2 (%)	τ_2 (ns)	τ_{ave} (ns)
293	69.29	5.02	30.71	32.15	25.08
303	69.53	5.34	30.47	34.57	26.95
313	68.44	5.06	31.56	35.78	28.57
323	66.90	4.62	33.10	35.37	28.95
333	67.73	4.47	32.27	35.94	29.43
343	67.79	3.34	32.21	31.78	26.63
353	71.49	2.78	28.51	28.01	22.98
363	74.88	2.23	25.12	21.15	16.63
373	77.76	2.11	22.24	18.02	13.40

Table S8. The fitting parameters of the decay curves for $CsPbBr_3$-SO_4 NCs at increasing temperature from 293 to 373 K.

Temperature / K	A_1 (%)	τ_1 (ns)	A_2 (%)	τ_2 (ns)	τ_{ave} (ns)
293	71.90	7.24	28.10	33.92	24.50
303	68.65	6.79	31.35	31.24	23.36
313	70.77	7.43	29.23	34.11	24.90
323	70.98	7.22	29.02	33.67	24.57
333	70.59	7.34	29.40	34.09	24.98
343	64.44	6.59	35.56	31.92	25.02
353	65.75	6.62	34.25	34.60	27.08
363	68.44	7.30	31.56	37.98	28.95
373	68.87	7.07	31.13	38.78	29.66

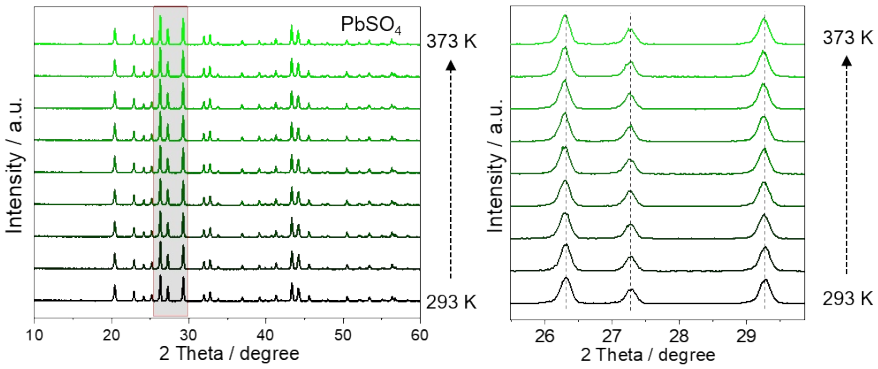

Figure S8. *In situ* XRD patterns of pure $PbSO_4$ sample at increasing temperature from 293 to 373 K.

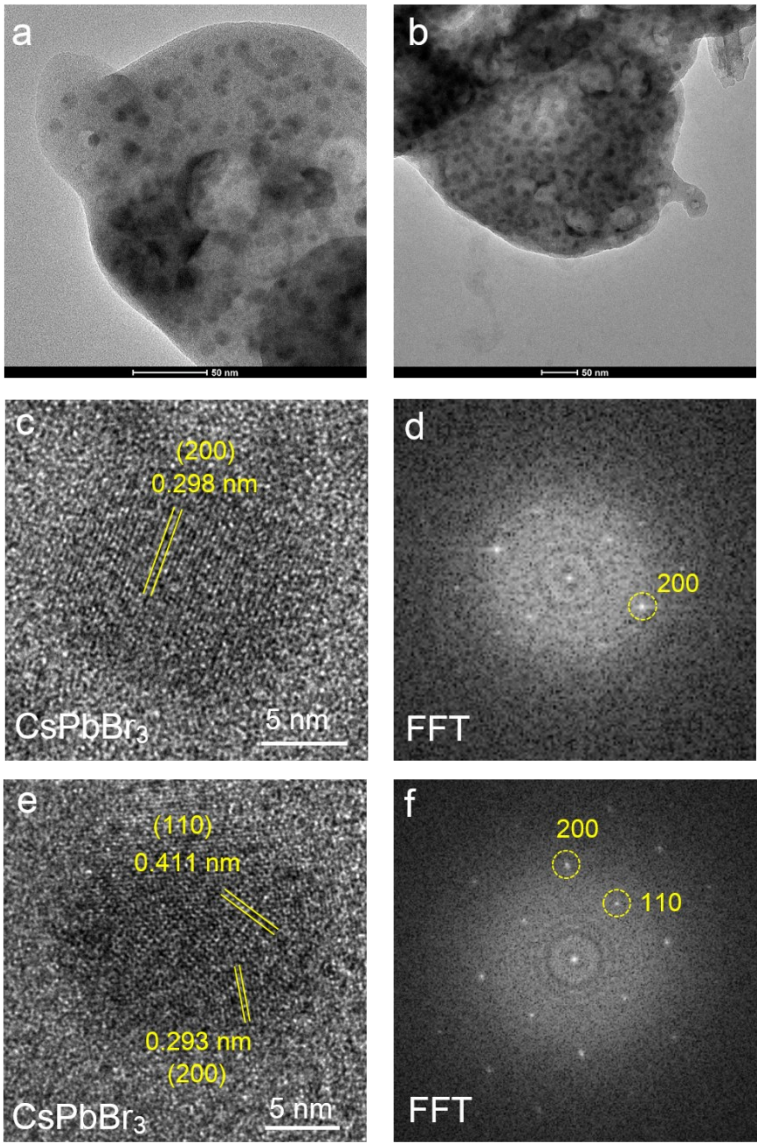

Figure S9. (a-b) TEM images of pristine $CsPbBr_3$ NCs. (c-f) HR-TEM images and the corresponding FFT images of pristine $CsPbBr_3$ NCs.

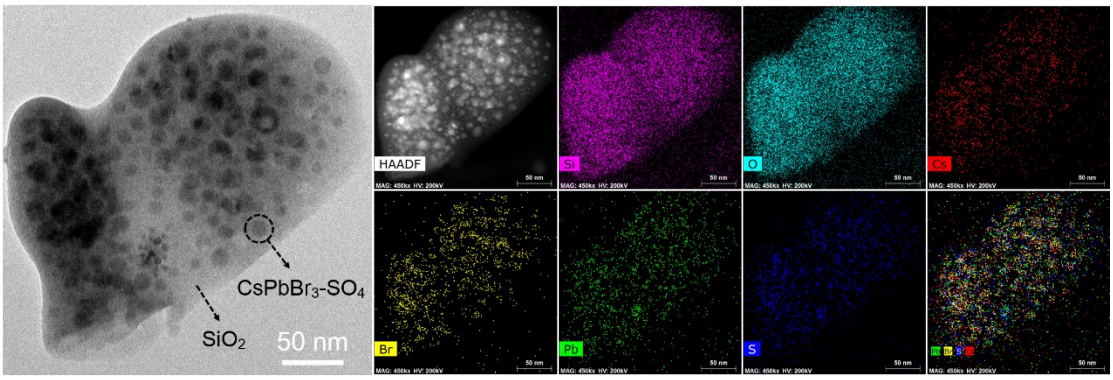

Figure S10. HAADF-STEM images of $CsPbBr_3$-SO_4 sample, and the corresponding elemental mapping of Cs, Pb, Br, O, Si, S.

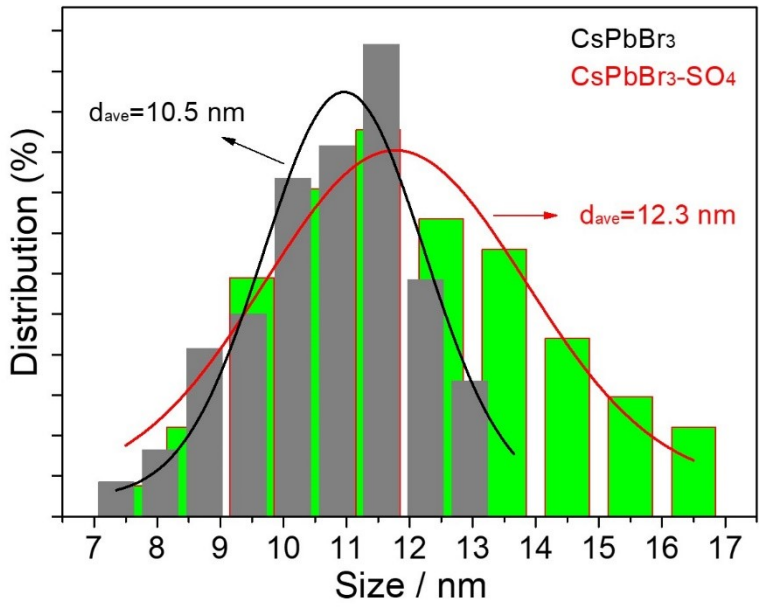

Figure S11. Size distributions of pristine and SO_4^{2-}-treated $CsPbBr_3$ NCs obtained from Figure S9 and Figure S10.

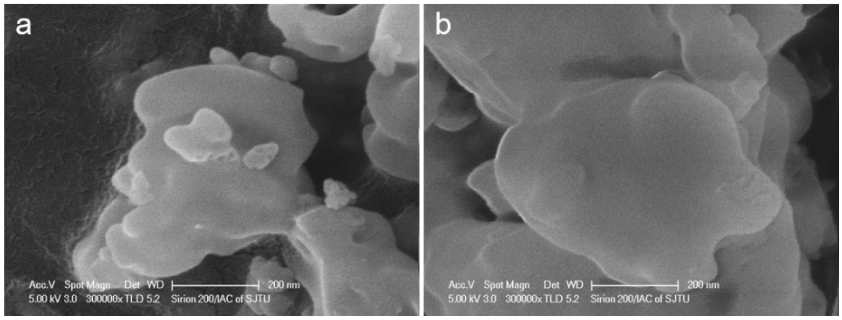

Figure S12. (a-b) SEM images of SO_4^{2-}-treated $CsPbBr_3$ NCs.

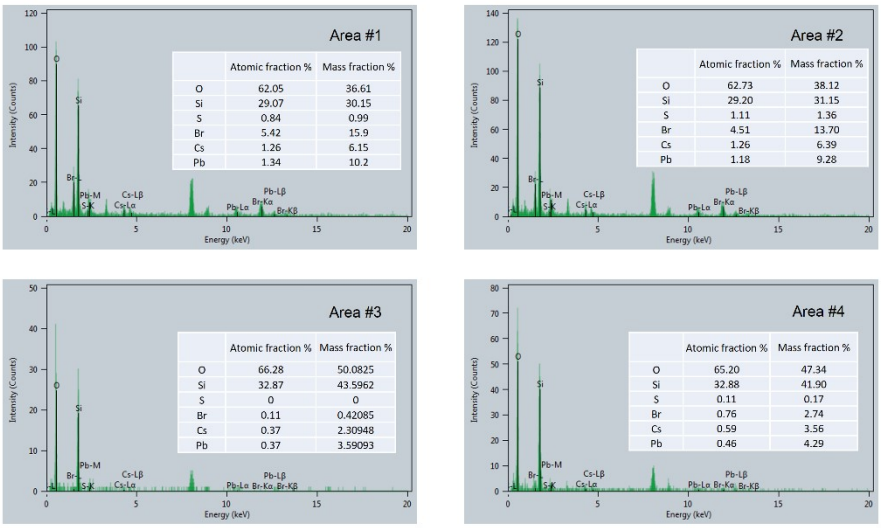

Figure S13. EDS scans of areas #1-4 indicated in Figure 4c-d.

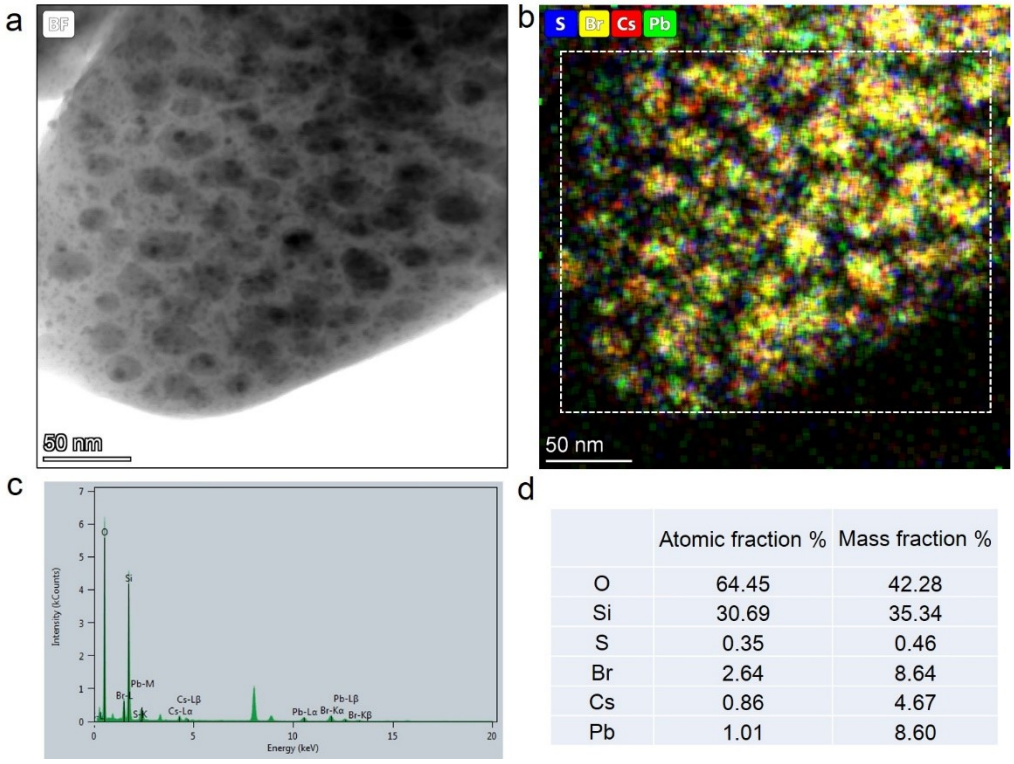

	Atomic fraction %	Mass fraction %
O	64.45	42.28
Si	30.69	35.34
S	0.35	0.46
Br	2.64	8.64
Cs	0.86	4.67
Pb	1.01	8.60

Figure S14. (a-b) TEM images of $CsPbBr_3$-SO_4 sample, and the corresponding elemental mapping. (c-d) EDS scans of the whole area indicated in Figure S14b.

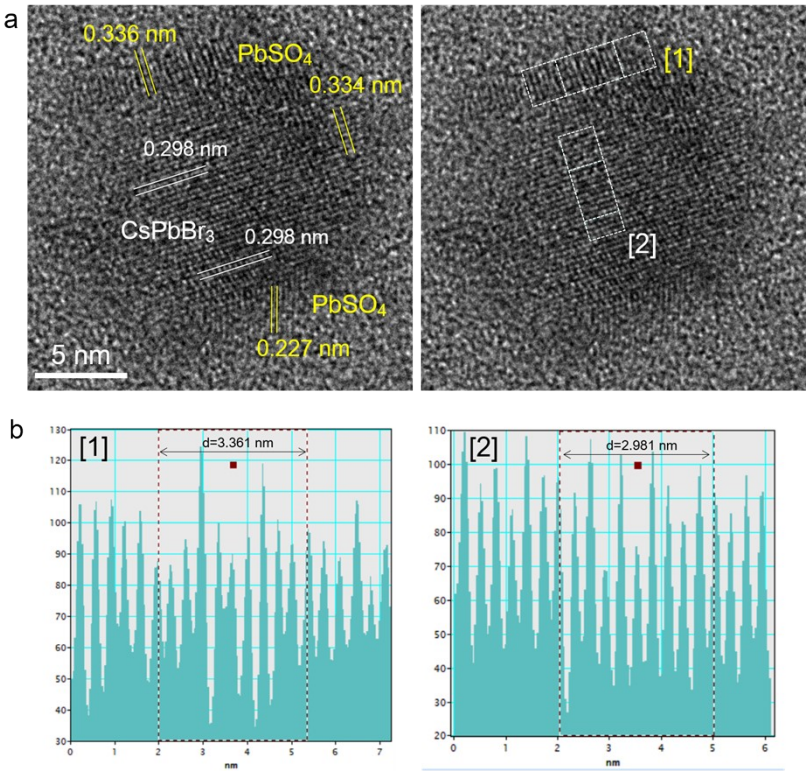

Figure S15. (a-b) HR-TEM images and the interplanar spacing vs. layer position of the whole set of analyzed SO_4^{2-}-treated $CsPbBr_3$ NCs.

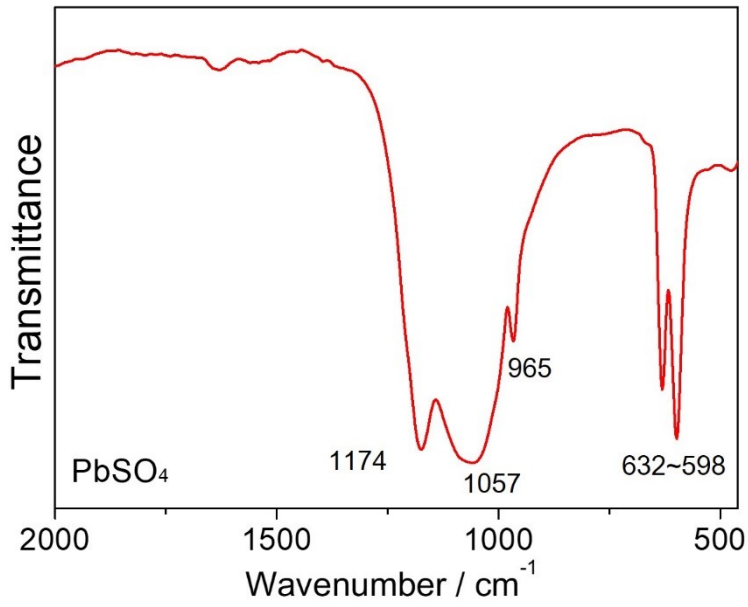

Figure S16. FT-IR measurement of pure $PbSO_4$ standard sample.

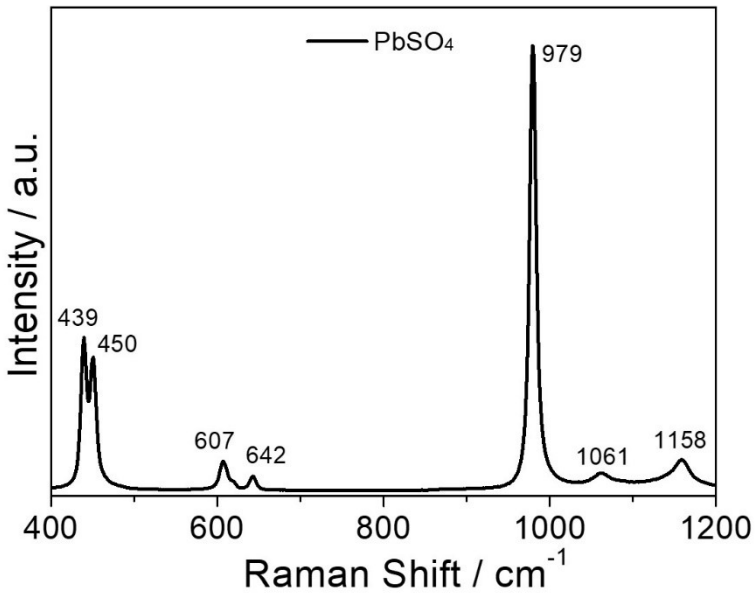

Figure S17. Raman spectra of $PbSO_4$ powder.

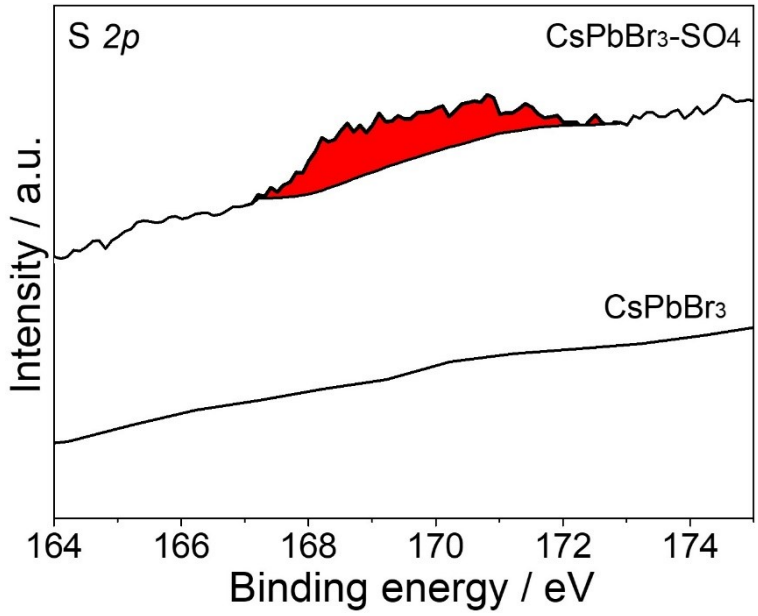

Figure S18. XPS spectra of S 2p for pristine and SO_4^{2-}-treated $CsPbBr_3$ NCs.

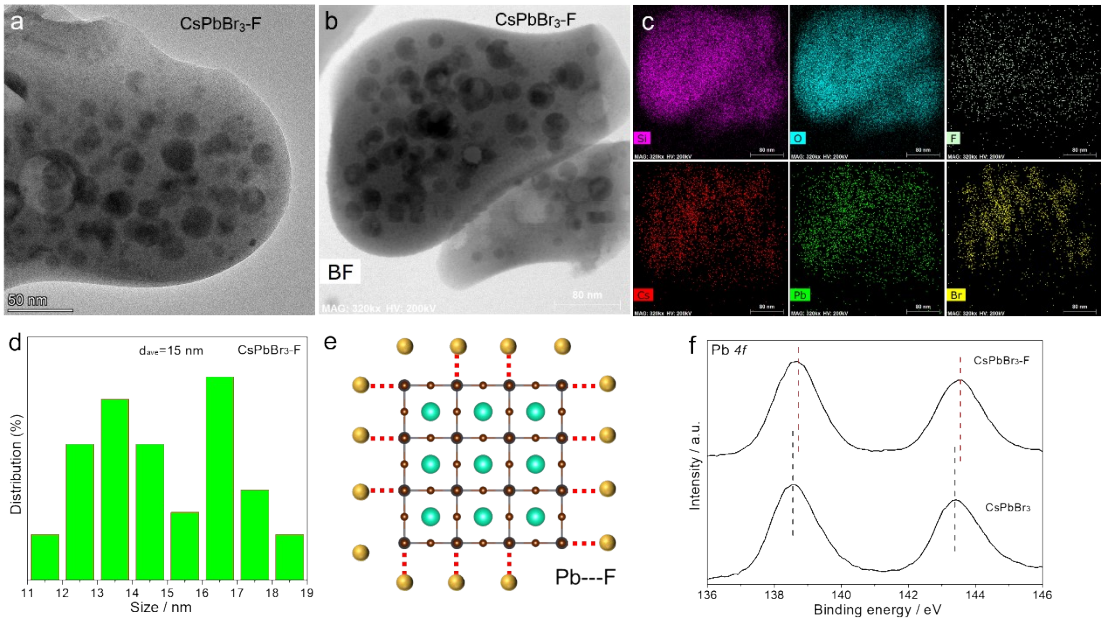

Figure S19. Structural studies for $CsPbBr_3$-F samples. (a, b) TEM images of $CsPbBr_3$-F samples. (c) The corresponding elemental mapping of Cs, Pb, Br, O, Si, F from Figure S12b. (d) Size distributions of F-treated $CsPbBr_3$ NCs. (e) Schematic diagram of the $CsPbBr_3$-F core-shell like structure. (f) XPS spectra of Pb 4f for pristine and F-treated $CsPbBr_3$ NCs.

Notes: From Figure S19a-c, the TEM images and corresponding elemental mappings of $CsPbBr_3$-F samples revealed that the Cs, Pb, Br, F elements were clearly distributed in the $CsPbBr_3$ NCs, indicating the F ions were adsorbed on the $CsPbBr_3$ NCs. Meanwhile, size distributions (Figure S19d) showed that fluorine treatment can effectively increase the size of $CsPbBr_3$ NCs from initial 10 nm to 15 nm, indicating the formation of shells (as shown in Figure S19e). Finally, after fluorine treatment, the Pb peaks of $CsPbBr_3$-F NCs shifted toward the higher binding energies, indicating the formation of stronger chemical bond between Pb^{2+} and F^- ions (Figure S19f).

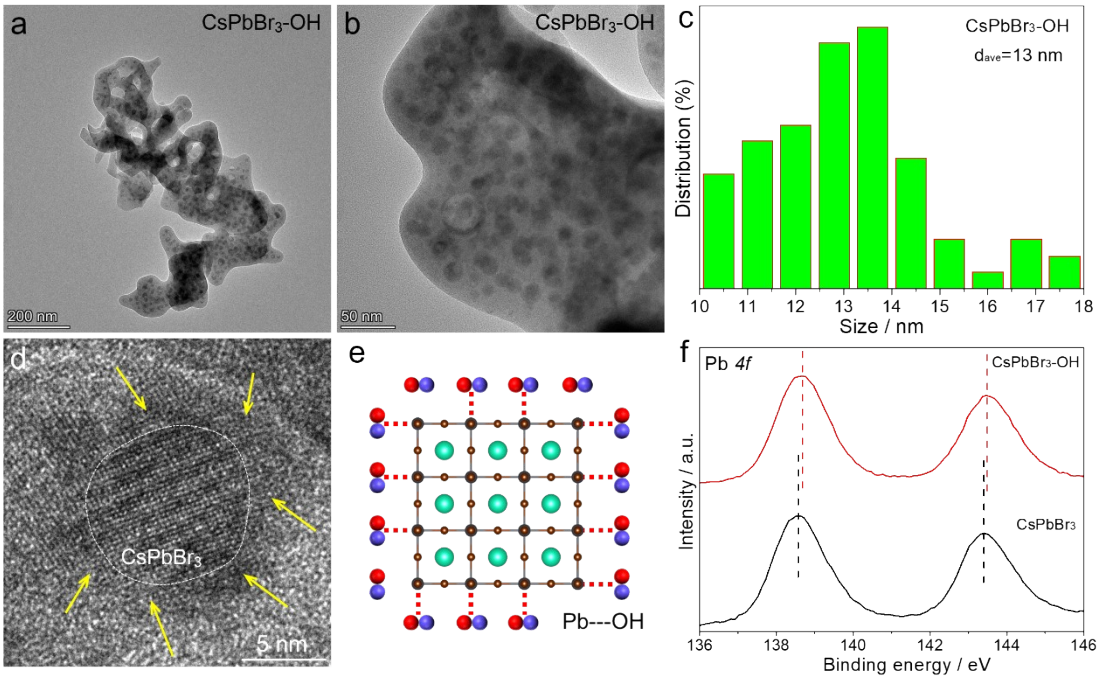

Figure S20. Structural studies for $CsPbBr_3$-OH samples. (a-b) TEM images of $CsPbBr_3$-OH samples. (c) Size distributions of OH-treated $CsPbBr_3$ NCs. (d) HR-TEM image of $CsPbBr_3$-OH NCs. (e) Schematic diagram of the $CsPbBr_3$-OH core-shell like structure. (f) XPS spectra of Pb 4f for pristine and OH-treated $CsPbBr_3$ NCs.

Notes: From Figure S20a-c, after OH^- treatment, size distributions showed that OH^- treatment can effectively increase the size of $CsPbBr_3$ NCs from initial 10 nm to 13 nm, indicating the formation of shells. In Figure S20d-e, HR-TEM image further revealed a uniform and compact layer that was tightly coated on the surface of $CsPbBr_3$ NCs, constructing a typical core-shell-like structure. Finally, after OH^- treatment, the Pb peaks of $CsPbBr_3$-OH NCs also shifted toward the higher binding energies, indicating the formation of stronger chemical bond between Pb^{2+} and OH^- ions (Figure S20f).

Table S9. The color coordinate of the WLED based on pristine $CsPbBr_3$ NCs at increasing temperature from 293 to 373 K.

Temperature / K	x	y
293	0.3309	0.3561
303	0.3339	0.3549
313	0.3406	0.3447
323	0.3447	0.3383
333	0.3500	0.3290
343	0.3587	0.3126
353	0.3679	0.2978
363	0.3736	0.2697
373	0.3756	0.2469

Table S10. The color coordinate of the WLED based on $CsPbBr_3$-SO_4 NCs at increasing temperature from 293 to 373 K.

Temperature / K	x	y
293	0.3463	0.3468
303	0.3487	0.3444
313	0.3494	0.3404
323	0.3517	0.3391
333	0.3536	0.3374
343	0.3563	0.3317
353	0.3621	0.3236
363	0.3655	0.3167
373	0.3676	0.3130

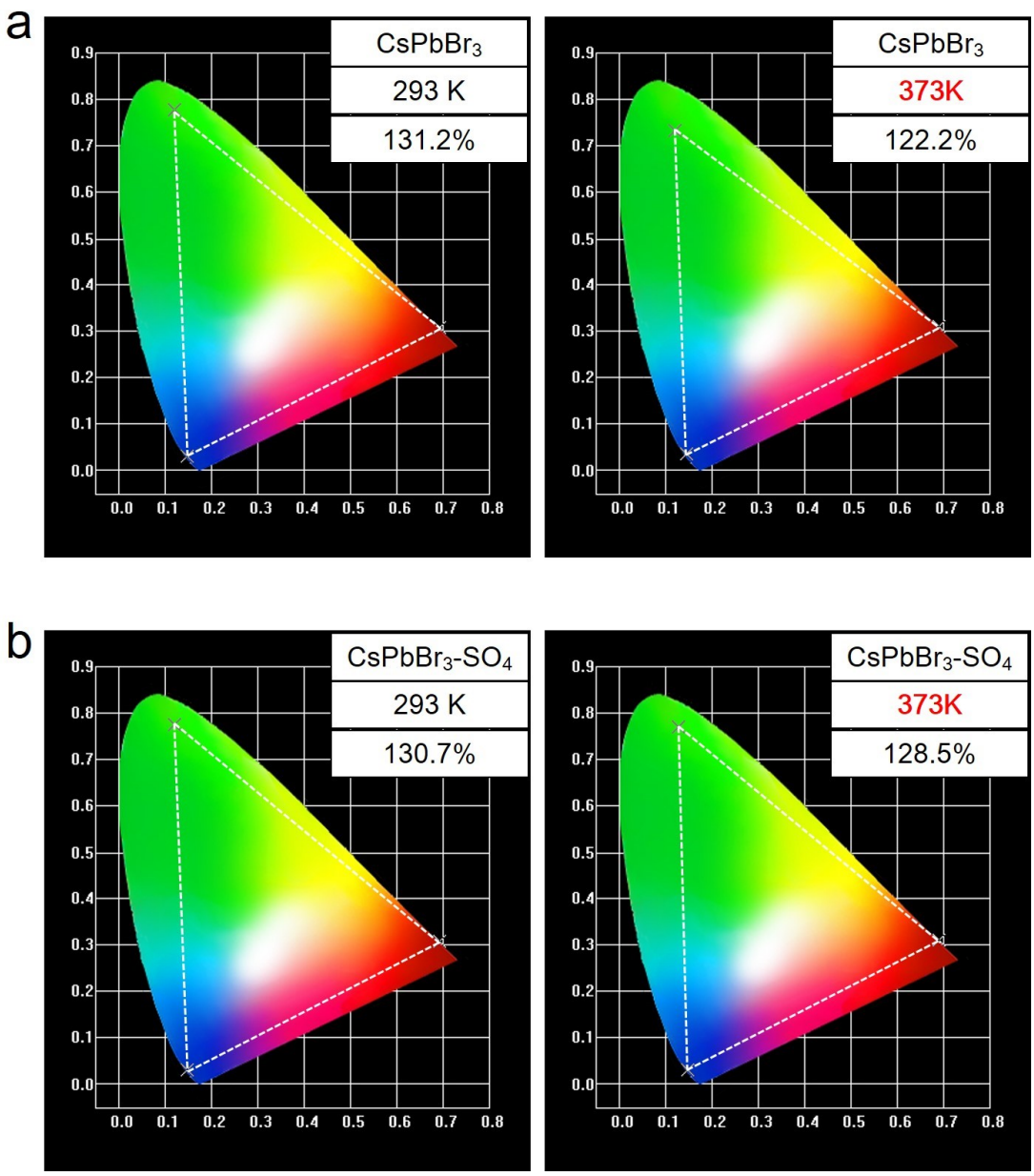

Figure S21. (a) The color gamut of the WLED devices based on $CsPbBr_3$ NCs at 293 K and 373 K. (b) The color gamut of the WLED devices based on $CsPbBr_3$-SO_4 NCs at 293 K and 373 K.

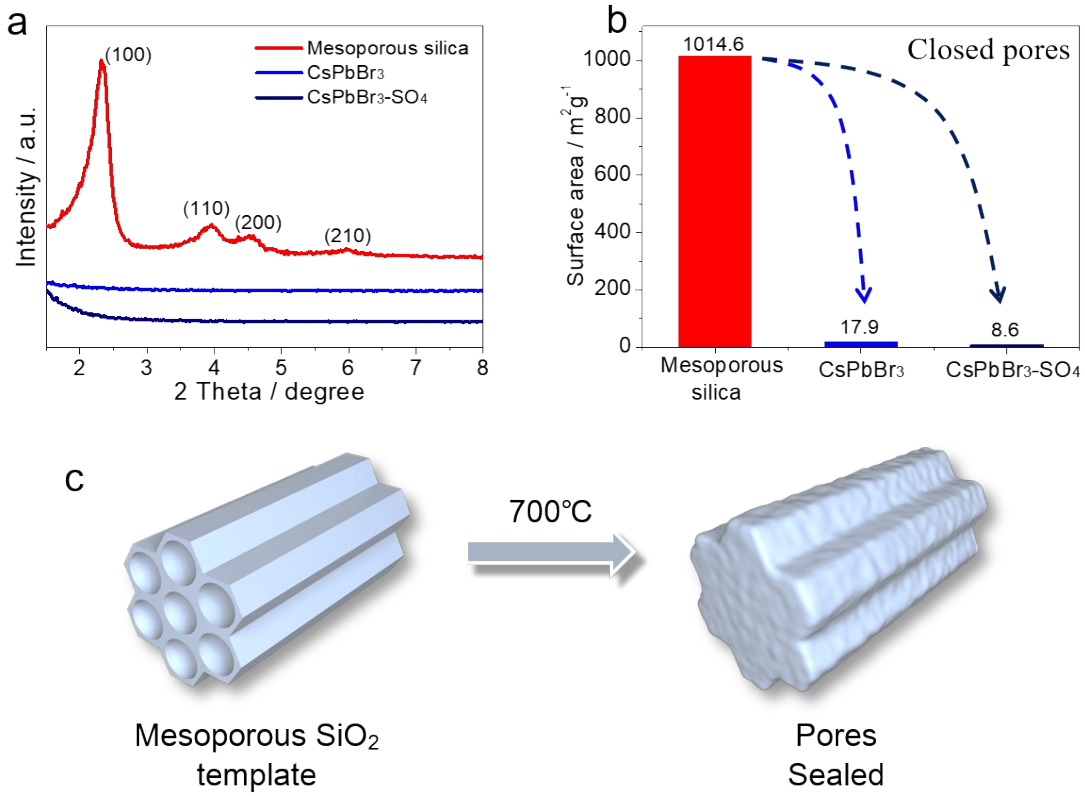

Figure S22. (a) Small-angle XRD patterns of original mesoporous silica, pristine $CsPbBr_3$ NCs, and SO_4^{2-}-treated $CsPbBr_3$ NCs. (b) Surface area of original mesoporous silica, pristine $CsPbBr_3$ NCs, and SO_4^{2-}-treated $CsPbBr_3$ NCs. (c) Schematic diagram of mesoporous silica collapse process.

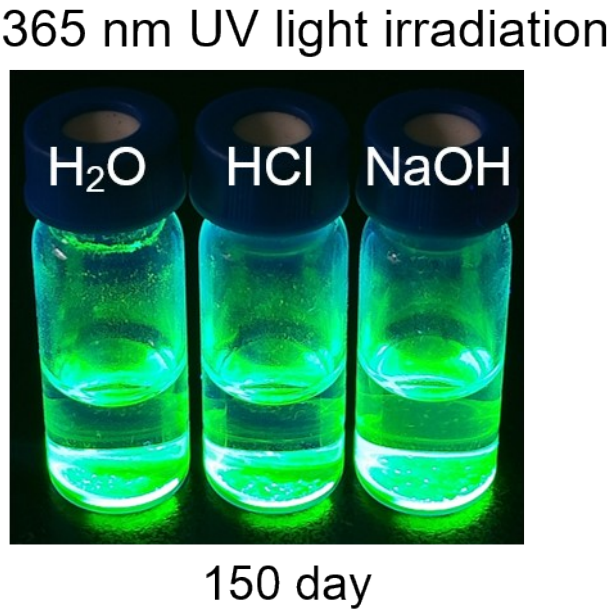

Figure S23. Photographs of $CsPbBr_3$-SO_4 NCs immersed in H_2O, immersed in 1M HCl solution, immersed in 0.1M NaOH solution for 150 days, under UV illumination.

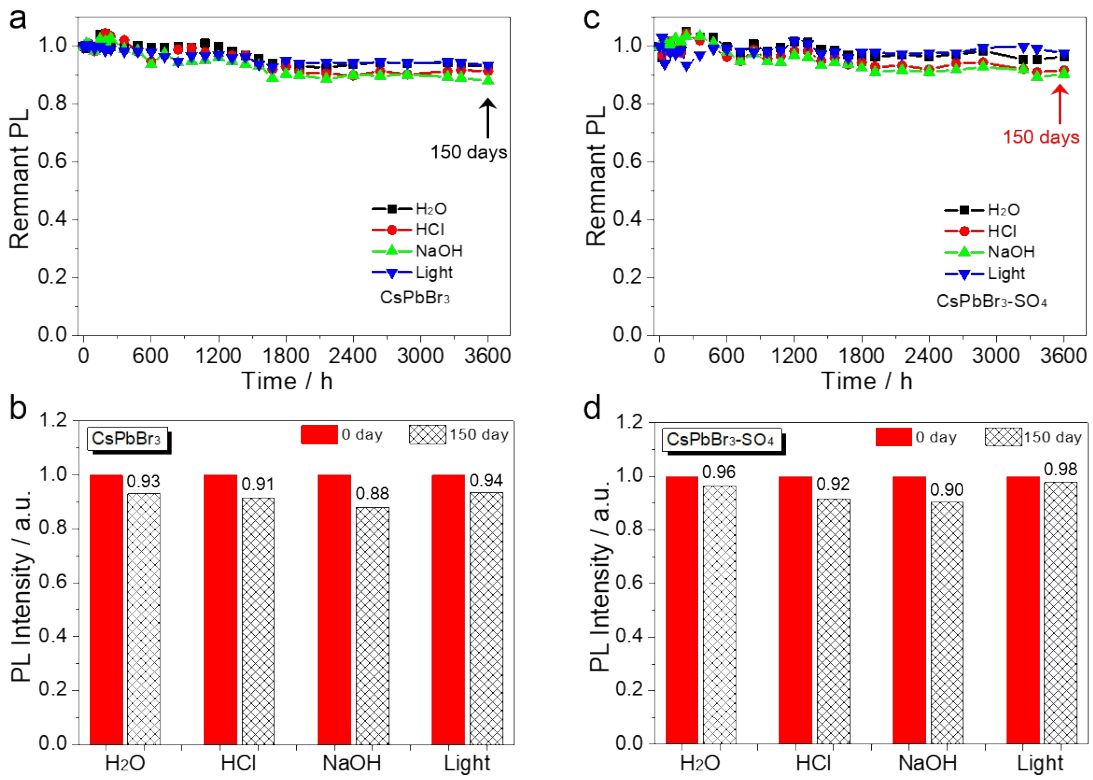

Figure S24. (a-b) Stability tests: the remnant PL of pristine $CsPbBr_3$ NCs after immersed in H_2O, in 1M HCl solution, in 0.1M NaOH solution, under continuous illumination with a 450 nm LED (350 mW cm^{-2}) for various times. (c-d) Stability tests: the remnant PL of $CsPbBr_3$-SO_4 NCs after immersed in H_2O, in 1M HCl solution, in 0.1M NaOH solution, under continuous illumination with a 450 nm LED (350 mW cm^{-2}) for various times.

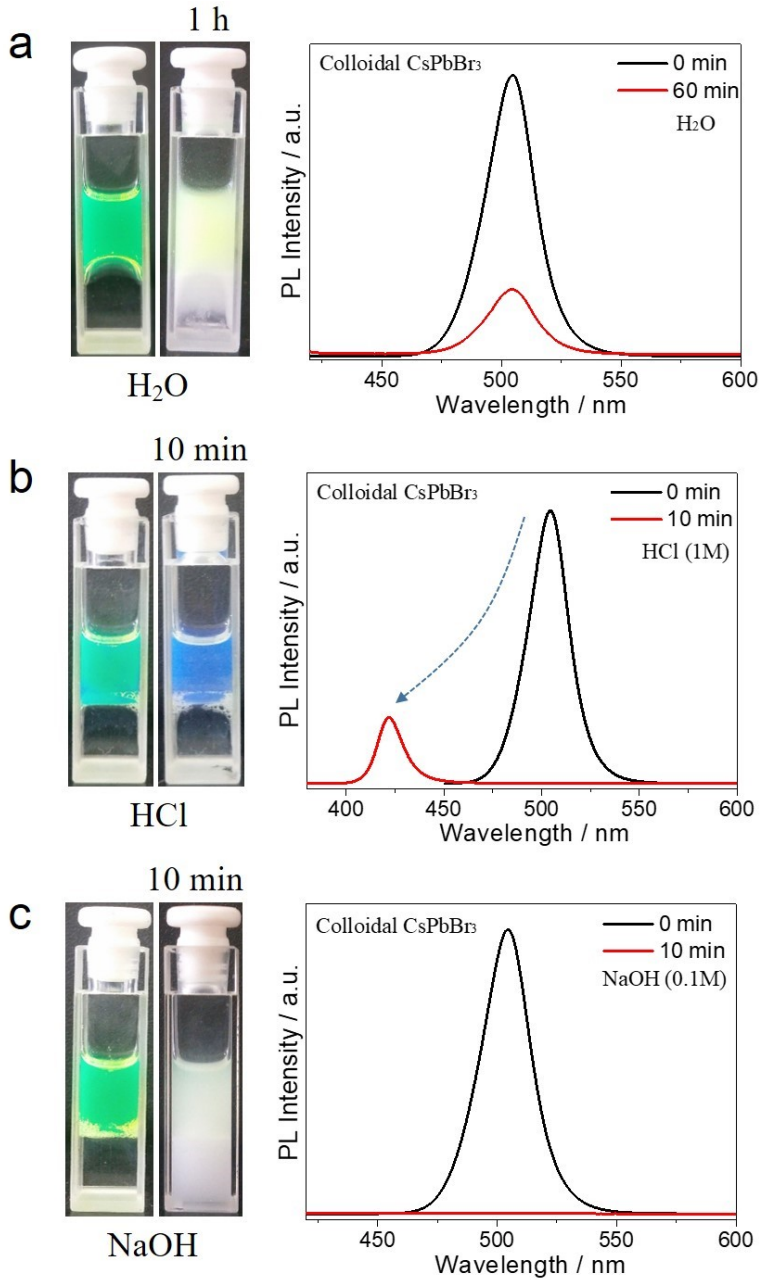

Figure S25. (a) Water resistance: photographs and PL spectra of colloidal $CsPbBr_3$ NCs immersed in H_2O for 1h. (b) Acid resistance: photographs and PL spectra of colloidal $CsPbBr_3$ NCs immersed in 1M HCl solution for 10 min. (c) Alkali resistance: photographs and PL spectra of colloidal $CsPbBr_3$ NCs immersed in 0.1M NaOH solution for 10 min.

Water stability, chemical stability, and photostability

Although the construction of wide-bandgap surface passivation layer can effectively weaken the high temperature induced thermal quenching behavior of $CsPbBr_3$ NCs in practical application, other factors, such as light irradiation and moisture, also threaten the stability of $CsPbBr_3$ NCs. As we previously reported, thanks to the unique encapsulation advantages based on a strategical collapse of mesoporous silica in the high-temperature solid-state method, the above stability problems have also been properly solved. Next, small-angle XRD patterns and surface area were performed to confirm the collapse of the pore structures of mesoporous silica at high temperature, as shown in **Figure S22**. For both pristine and SO_4^{2-}-treated $CsPbBr_3$ NCs, with the increase of calcination temperature up to 700 ℃, the intensities of the major peaks from the pore structures decreased rapidly (**Figure S22a**), and the surface area of target samples sharply decreased from 1014.6 m^2g^{-1} to 8.6 m^2g^{-1} (**Figure S22b**), meaning that mesoporous silica had collapsed completely at 700 ℃ and the $CsPbBr_3$ NCs were encapsulated into the compact SiO_2 solid during the collapse process. Due to the dense SiO_2 encapsulation, the obtained $CsPbBr_3$ NCs exhibited ultra-high stability against water, strong acid, strong base, and light irradiation. As shown in **Figure S23-24**, no obvious PL emission decays were observed for encapsulated $CsPbBr_3$ NCs under harsh environments (water, 1M HCl, 0.1M NaOH, illumination with a 450 nm LED) over 3600 h, showing excellent water stability, chemical stability, and photostability, which was far superior to traditional colloidal $CsPbBr_3$ NCs (rapidly decays within 1 hour in **Figure S25**). Owing to anions passivation and high-temperature encapsulation strategy, the obtained $CsPbBr_3$ NCs not only effectively suppress their thermal quenching behavior, but also achieve a breakthrough in the stability of light and moisture, which have great potential in the practical display application in the future.